Mechanical energy transfer and dissipation in fibrous beta-sheet-rich proteins

Zhiping Xu[1] and Markus J. Buehler[1,2,*]

[1]*Laboratory for Atomistic and Molecular Mechanics, Department of Civil and Environmental Engineering,
Massachusetts Institute of Technology, 77 Massachusetts Avenue, Room 1-235 A&B, Cambridge, Massachusetts 02139, USA*
[2]*Center for Computational Engineering, Massachusetts Institute of Technology,
77 Massachusetts Avenue, Cambridge, Massachusetts 02139, USA*

Mechanical properties of structural protein materials are crucial for our understanding of biological processes and disease states. Through utilization of molecular simulation based on stress wave tracking, we investigate mechanical energy transfer processes in fibrous beta-sheet-rich proteins that consist of highly ordered hydrogen bond (H-bond) networks. By investigating four model proteins including two morphologies of amyloids, beta solenoids, and silk beta-sheet nanocrystals, we find that all beta-sheet-rich protein fibrils provide outstanding elastic moduli, where the silk nanocrystal reaches the highest value of ≈ 40 GPa. However, their capacities to dissipate mechanical energy differ significantly and are controlled strongly by the underlying molecular structure of H-bond network. Notably, silk beta-sheet nanocrystals feature a ten times higher energy damping coefficient than others, owing to flexible intrastrand motions in the transverse directions. The results demonstrate a unique feature of silk nanocrystals, their capacity to simultaneously provide extreme stiffness and energy dissipation capacity. Our results could help one to explain the remarkable properties of silks from an atomistic and molecular perspective, in particular its great toughness and energy dissipation capacity, and may enable the design of multifunctional nanomaterials with outstanding stiffness, strength, and impact resistance.

I. INTRODUCTION

Fibrous proteins such as amyloid fibrils, beta-solenoid protein nanotubes, and beta-sheet nanocrystals as found in spider and insect silks have attracted great interest because of their physiological function, pathological relevance, as well as their potential to provide insights toward novel material design [1,2]. These biological fibers are usually exposed to dynamical environments such as rapid loading during prey procurement, injuries, or fluctuating pressure and temperature conditions. Therefore, the understanding of mechanical energy flow is the key to elucidate material mechanisms relevant for physiological and disease states. The molecular structures of amyloid fibrils, beta-solenoid protein nanotubes, and silk nanocrystals all consist predominantly of beta-sheet secondary protein structures [Figs. 1(a)–1(f)].

In fact, beta-sheet-rich protein structures are universally found protein structures that are accessible to polypeptide chains with greatly variegated amino acid sequences [3]. Experimental and simulation investigations reveal remarkable structural stability and mechanical resistance against mechanical, thermal, and chemical perturbations from environments [4–6]. However, unlike engineering materials such as metal and glasses that rely on strong (e.g., metallic or covalent, ≈ 100 kcal/mol and more) bonds, the high stiffness of beta-sheet-rich protein materials is achieved by exceedingly weak intermolecular forces such as H bonds and hydrophobic interactions. Yet, despite the weakness of H bonds (with typical bond energies on the order of ≈ 5 kcal/mol), it has

been shown that beta-sheet-rich protein materials display great moduli approaching 40 GPa. As a striking example, spider silk features an extremely high level of strength (approaching that of steel), toughness, and extensibility of tens of percent strain, as well as an enormous capacity to dissipate mechanical energy [7].

Recent work has shown that these properties must be understood based on the structural hierarchies found in biological materials, which range from H-bond networks to the overall cellular or tissue scale [8]. As was demonstrated in recent experimental studies [9,10], the particular nanostructure found in these materials can be crucial in determining their macroscale properties. Yet, fundamental issues related to mechanical properties of key protein constituents such as beta-sheet-rich building blocks remain unknown, in particular their response to extreme mechanical loading in the context of mechanical energy transfer and dissipation. Here, we address this issue by using atomistic simulation that provides a bottom-up material description, which enables a systematic comparison of the mechanical energy transfer and dissipation capacity of different fibrous beta-sheet-rich proteins.

II. MATERIALS AND METHODS

In order to gain insight into the mechanical energy transfer process in fibrous proteins, we propose a stress wave-front tracking (WFT) approach. This approach, complementary to the widely used steered molecular-dynamics (SMD) method and atom force microscopy measurements, provides detailed structural and dynamical information of mechanical properties and energy transport from a molecular perspective. Importantly, it rules out ambiguous issues such as loading rate dependence and deformation localization at the load-

───────

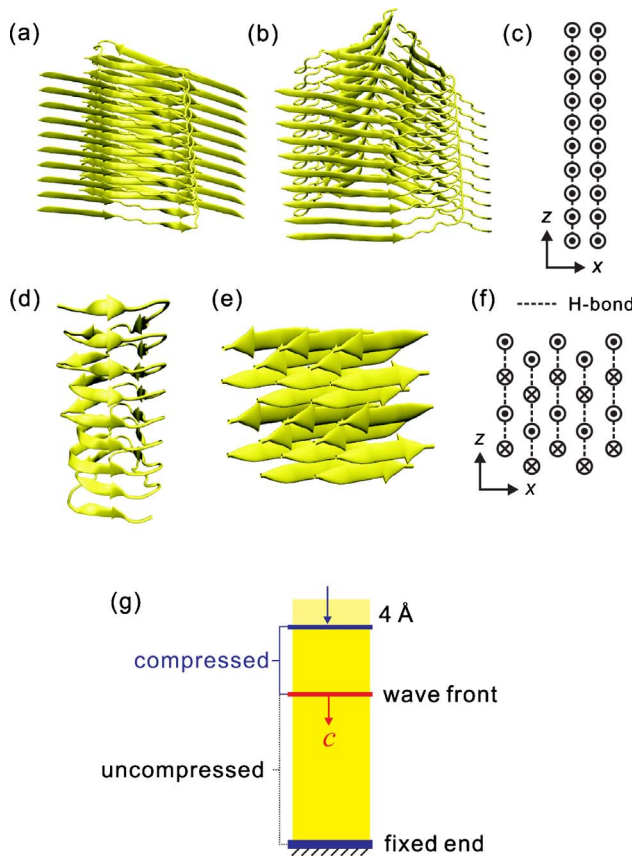*Corresponding author. FAX: +1-617-324-4014;
mbuehler@mit.edu

FIG. 1. (Color online) Beta-sheet-rich proteins investigated, and schematic of loading condition. (a) Twofold $A\beta(1-40)$ amyloid fibrils with a cross-beta structure. Each protofibril layer comprises of a peptide chain dimer. (b) Threefold $A\beta(1-40)$ amyloid fibrils, where three beta strands form a hydrophobic pore. Panel (c) shows the amyloid fibril structure as a schematic one-dimensional H-bond chain. (d) Beta-solenoid protein with both cross-beta structure and continuous covalent bonds throughout the backbone. (d) Antiparallel beta-sheet nanocrystal, resembling the crystalline domain in spider silk. (e) An illustration of the silk nanocrystal as a two-dimensional lattice with beta sheets arranged in parallel. To visualize the molecular structure, only parts of the fibrils (ten-layer amyloid fibrils, nine loops in beta solenoid, and four layers in the silk nanocrystal) used in the simulations are shown here. (g) Schematic of the loading condition used in the wave-front tracking (WFT) approach.

ing boundaries [11,12] (both limitations of the conventional SMD approach and related methods), and as such provides a powerful tool toward understanding mechanical energy transfer processes at the nanoscale.

In the WFT approach, a displacement-based compressive pulse load (with an amplitude of $d=0.4$ nm and speed of $v_0=100$ m/s) is applied to one end of the fibrous protein at the beginning of the simulation [Fig. 1(g)]. A small value of d is required to maintain linear elasticity. The elastic stress wave propagation is tracked subsequently after removing the pulse load and keeping both ends fixed. The averaged center-of-mass position of C_α atoms $u(t)$ in each protofibril is recorded as a function of time t, to track the position of the stress wave font (defined as the boundary between deformed and undeformed regions). According to the extracted stress

wave-front speed c, we obtain the axial Young's modulus Y of the fibril through [13]

$$Y = c^2\rho, \qquad (1)$$

where ρ is the mass density of fibrous proteins, calculated from the total atomic mass and geometric parameters as introduced below. To validate the WFT method, the Young's modulus of ice (in hexagonal Ih phase [14]) along the $\langle 0001 \rangle$ direction is calculated. The result of $Y=8.25$ GPa is in good agreement with the experimental measurement of 8.6 GPa along the same crystallographic orientation [14].

Here, we consider both parallel and antiparallel beta-sheet structures. Three types of fibrous proteins containing *parallel* beta-sheet structures are investigated here, including twofold and threefold $A\beta(1-40)$ amyloid fibrils, as well as a beta-solenoid protein [see Figs. 1(a), 1(b), and 1(d)]. Amyloid fibrils are associated with a number of diseases including Alzheimer and prion diseases, with a characteristic twisted layered cross-beta structure [15,16]. The twofold fibril consists of 60 protofibril layers with total length $L=28.91$ nm. It has a rectangular cross section with height $h=2.874$ nm and width $w=4.667$ nm. This configuration enables a close contact between two hydrophobic peptide chains in each layer. In the 60-layer threefold fibril ($L=29.1$ nm), three beta strands form a circular cross-beta motif, leaving a hydrophobic core at the inside of the tube structure. The cross section is an equilateral triangle with edge length $a=6.47$ nm. The underlying H-bond network density D_{HB} in these two amyloidic structures is 1.3 H bonds per residue. In addition to $D_{HB}=1$ H bond per residue from the backbone [17], side chains also contribute to the overall H-bond density. The third parallel beta-sheet protein considered here is a beta solenoid with $D_{HB}=1.1$ H bonds per residue, a nanotubular protein that can be found in the cell puncture needle of bacteriophage T4 virus. The molecular structure investigated here has a diameter of $d=3$ nm and length of $L=39.5$ nm. On top of the H bonds, the connected backbone throughout the fibril provides additional mechanical resistance to axial load at large deformation.

Antiparallel beta sheets, as found in crystalline domain of spider and insect silks, have also been associated with impressive mechanical properties. In cooperation with the resilient domains that include more disordered chains, beta-sheet nanocrystals provide simultaneously high strength and toughness to silk materials [5,6,18]. Here, we consider a silk II polymorph nanocrystal of *B. mori* as depicted in Fig. 1(e) [19]. Six-residue short polypeptides [polyglycine-alanine, $(GA)_3$] stack into a two-dimensional crystal with a H-bond density $D_{HB}=1$ H bond per residue and interstrand distance $d=0.4$ nm. A 32×8 superlattice (32 layers along fibril axis and eight parallel strands in the cross section) of the polypeptides is constructed to form the beta-sheet nanocrystal.

In the molecular-dynamics simulation approach we employ the CHARMM19 all-atom energy function for proteins and an effective Gaussian model for the water solvent [20,21] to facilitate rapid sampling of structural configurations [22]. The structures of amyloid, beta-solenoid proteins, and silk nanocrystals are energy minimized in explicit sol-
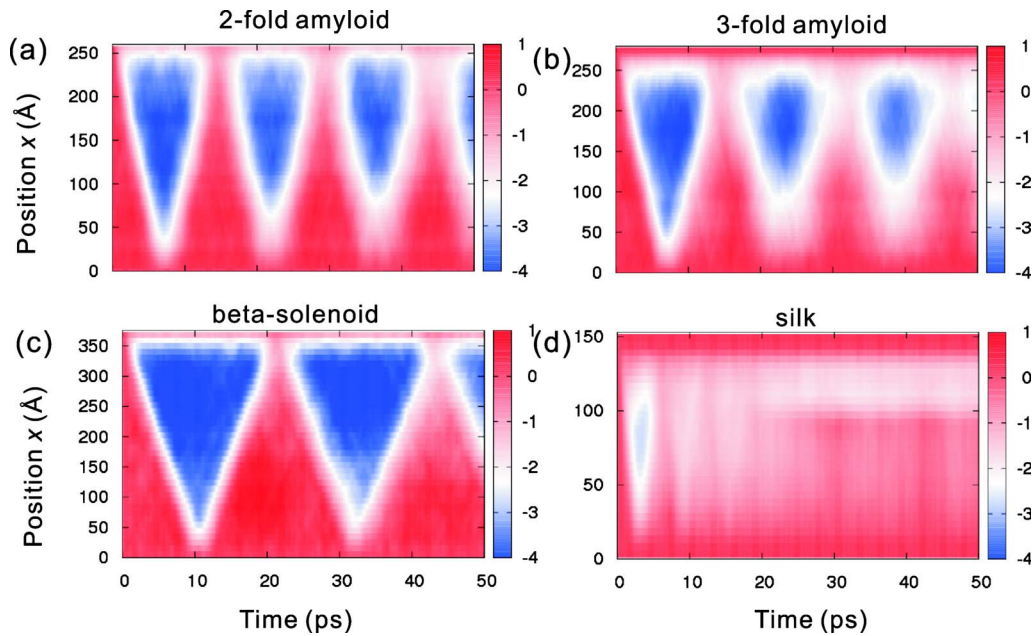
FIG. 2. (Color online) Axial displacement of constituting protofibrils obtained from the wave-front tracking approach. In comparison with amyloid fibrils (a) and (b), the compressive wave in the beta-solenoid protein (c) features less energy dissipation due to the backbone along the axial direction. In the silk nanocrystal (d), transverse flexibility introduces severe damping and the wave propagation decays rather quickly.

vent following experimental structure identification and then moved to the effective Gaussian solvent model. As the internal H-bond network (which is not exposed to water solvent) determines the mechanical response of fibrous proteins, we expect that there is a relatively small difference between our approach and explicit solvent treatment. For the ice crystal, the TIP3P model [23] is used to model water molecules.

In all simulations, an equilibration process at 300 K is carried out for 500 ps before the compressive pulse load is applied. All dynamical simulations including the loading and tracking process are performed under an NVT ensemble at $T = 300$ K. We use Nosé-Hoover thermostat with an integration time step of 1 fs. In order to observe a distinct wave propagation feature, the displacement-based loading is applied with a rather large speed, i.e., on the order of 100 m/s. However, when the loading rate exceeds sound speeds, the tested protein fiber starts to fail and the H-bond network will be broken. To avoid an inelastic response of protein materials, we use different speeds for the pulse load in the range from 10 to 1000 m/s and confirm that they do not alter the material properties extracted from the simulation. For the results presented here we choose $v_0 = 100$ m/s.

III. RESULTS AND DISCUSSION

A. Stress wave propagation

Figure 2 plots axial displacements $u(z, t)$ of all fibrous proteins considered (z direction points along the fibril axis). Stress wave characteristics such as propagation at a specific constant sound speed, reflection at the boundary, and energy dissipation are observed. The sharp and straight stress wave-front propagating as a function of time indicates that

deformation is in the linearly elastic regime. In the twofold and threefold amyloid fibrils, the observed group speeds are $c = 4000$ and 3860 m/s, corresponding to axial Young's moduli $Y = 27.24$ and 26.50 GPa, respectively. These values confirm previous experimental measurements [24] and atomistic level normal-mode analysis [25]. The agreement of Young's moduli in twofold and threefold amyloid fibrils results from the same cross-beta H-bond density (1.3 H bonds per residue) and similar mass density (1702.41 kg/m³ for twofold and 1778.64 kg/m³ for threefold structures). Their Young's moduli thus give a quantitative prediction for a broader class of proteins that share a similar parallel cross-beta structure. In the beta-solenoid protein, the backbone of the beta helix extends continuously throughout the fibril. Thus, under mechanical loading the propagation of mechanical energy could in principle be shared by deformation in both covalent bonds in backbone and H bonds aligning along the beta-helix axis. In this structure, the compressive wave speed $c = 3600$ m/s is lower than in the amyloid fibrils, probably due to the less compact H-bond network ($D_{HB} = 1.1$ H bonds per residue). Nevertheless, a comparable Young's modulus $Y = 26.37$ GPa is observed because the beta-solenoid protein has a more compact molecular structure, and the overall mass density of beta-solenoid protein is 2044.37 kg/m³, which is 15−20 % higher than in amyloid fibrils. Notably, this result shows that covalent bonds in the backbone do not have a significant contribution to wave dynamics, and that the strain energy is mostly absorbed by deformation of H-bond networks. For the silk nanocrystals with antiparallel beta sheets, the WFT simulation along the fibril axis yields a compressive wave speed of $c = 3600$ m/s and a Young's modulus of $Y = 39.36$ GPa. The Young's modulus estimated here is 30% higher than that of

TABLE I. Structural, elastic and dynamical properties (Young's modulus Y, relaxation time τ and H-bond density D_{HB}, and effective stiffness k_{HB} of H bonds) of the fibrous proteins investigated here (for images of the proteins, see Fig. 1).

Protein structure	Y (GPa)	τ (ps)	D_{HB} (No. of H bonds/residue)	k_{HB} (N/m)
Twofold amyloid fibril	26.50	10.19	1.3	8.14
Threefold amyloid fibril	27.24	8.04	1.3	7.40
Beta-solenoid protein	26.37	17.85	1.1	4.42
Silk nanocrystal	39.36	2.68	1.0	9.85

parallel beta sheets, and provides the largest value of all cases considered here.

To quantitatively relate the elastic properties to their protein structure, we consider a fibrous protein as a network where H bonds align parallel to their axes, as illustrated in Figs. 1(c) and 1(f). We can therefore define the Young's modulus Y based on an effective stiffness k_{HB} for individual H bond. For a one-dimensional network, as a strain ε is applied, we have axial force $F = YA\varepsilon = (N_{HB}/N_L)k_{HB}(L\varepsilon/N_L)$, where N_{HB} is the total number of H bonds in the network and N_L is the number of layers connected by H bonds in serial. This results in

$$k_{HB} = YAN_L^2/(N_{HB}L). \tag{2}$$

This effective stiffness k_{HB} of the H bond is renormalized in comparison to an isolated single H bond and additionally reflects the local environment, such as the cooperativity with neighboring H bonds. As summarized in Table I, we find that the two amyloid fibrils share similar k_{HB} values of 8.14 and 7.40 N/m. The k_{HB} value in the twofold structure is higher due to the interaction between protofibrils at the close contact interface, which is absent in the threefold structure as it is separated by the hydrophobic pore instead. The beta-solenoid has a lower value of 4.42 N/m. We find that the average H-bond length is greater in this case due to additional tension imposed by the backbone in comparison with amyloid fibrils. This elongation effectively weakens the stiffness of H bonds. The silk nanocrystal has a high value of $k_{HB} = 9.85$ N/m, reaching the highest value. As shown in Fig. 1(f), the silk nanocrystal has a two-dimensional face-centered lattice in the plane perpendicular to the peptide backbones. In addition to the antiparallel H bonds along the y direction, the interaction between adjacent beta sheets is responsible for the enhancement of the k_{HB} value. This is also reflected by the shorter H-bond lengths found in silk nanocrystals.

B. Energy dissipation

Another important finding derived from the data shown in Fig. 2 is that mechanical energy emitted from pulse loads begins to dissipate within the time scale of hundreds of picoseconds; however, the individual cases considered here feature a dramatically different behavior. In all cases, the main dissipation sources are viscous damping, converting stress wave energy into heat, and energy loss when the stress wave is reflected at the end, where the stress is multiplied [13]. The first mechanism characterizes intrinsic material properties and is determined by the hierarchical structure of H bonds in protein fibrils. The second mechanism is defined by the boundary condition rather than an intrinsic material property, which is confirmed by the blunt wave fronts.

Compared with amyloid fibrils and beta-solenoid proteins, the damping of compressive stress waves is much more severe in silk nanocrystals. To quantify the stress wave attenuation, we define the damping coefficient as $D = \Delta W/(WT)$ [13], where $W = Mv_{max}^2/2$ is the kinetic energy stored in the deformed material, M is the mass, and v_{max} is the maximum wave speed of the protofibril. T is the time period for a stress wave to cycle between two ends and ΔW is the kinetic energy loss within 1 cycle. By applying this definition to our results, that is, by fitting $v_{max}^2(t)$ with a function of the form $C\exp(-Dt)$, we obtain relaxation times $\tau = 1/D = 10.19$ and 8.04 ps for twofold and threefold amyloid fibrils, and 17.85 and 2.68 ps for beta-solenoid protein and silk nanocrystals, respectively.

While propagating, the energy carried by a mechanical stress wave is damped by internal friction from structural viscosity, i.e., by channeling kinetic energy of the axial stress wave into heat [13]. In thermal equilibrium, the protofibril exhibits thermal vibration around its equilibrium position, bound by a potential well produced by its neighbors. As compression is applied, the energy barrier is enhanced along protein fibril axis while reduced in the transverse direction. The stress wave energy is pumped into transverse motion of protofibrils in the protein, and subsequently to heat. The rate of energy dissipation depends on these channels that couple an effective continuum stress wave and the thermal vibration of individual atoms.

In our WFT simulation, we find that threefold amyloid fibrils have a larger damping coefficient than the twofold fibril. This is due to the fact that the hydrophobic pore in the threefold amyloid fibril features a greater flexibility than the close contact in the twofold amyloid fibril [25], while in the beta-solenoid protein transverse motion is restrained by the continuously (covalently bonded) backbone, and thus mechanical energy dissipates less. Impressively, the silk nanocrystal dissipates the mechanical wave much more efficiently than any of the other structures, as shown in Fig. 3. The relaxation time $\tau = 2.68$ ps is one order of magnitude lower than that of the beta solenoid. To explain the origin of this phenomenon, we plot the trajectory of protofibrils in Fig. 4, in terms of the relative displacements $(\Delta x, \Delta y)$ between one individual protofibil $(x_{protofibril}, y_{protofibril})$ and the average displacement of each layer (x_{layer}, y_{layer}) that describes the motions of the fibril. The data shown in Fig. 4 clearly show that in the twofold amyloid fibril, "continuum-type" beamlike bending modes of the fibril are excited, while in the silk nanocrystal we observe significant additional motion of beta strands in the transverse x and y directions. This energy coupling, involving an out-of-phase motion of protofibrils, accelerates energy dissipation drastically.

The high capacity to dissipate mechanical energy through flexible interstrand motion in silk nanocrystals paves the way
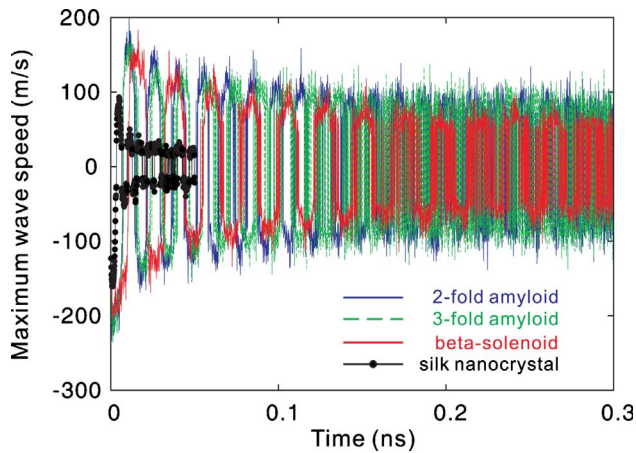
FIG. 3. (Color online) Attenuation of the maximum axial wave speed in various fibrous beta-sheet rich proteins. Internal friction defines a characteristic time scale τ (for an overview of numerical values, see Table I) before the mechanical wave energy (imposed by the loading) decays into thermal motion. The silk nanocrystal shows severe damping due to its flexibility and the emergence of transverse motion. In contrast, the beta-solenoid protein has the longest relaxation time due to the structural integrity imposed by its continuous and covalently bonded protein backbone.
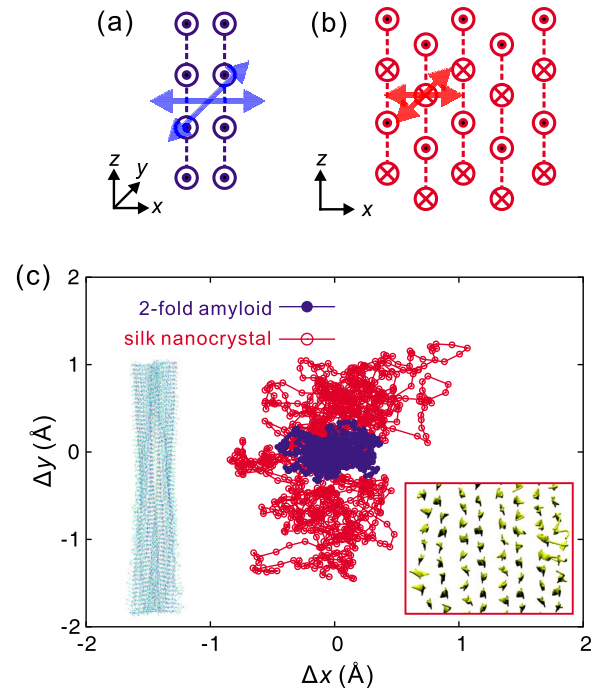

FIG. 4. (Color online) Trajectory of protofibrils in the twofold amyloid fibril and the silk nanocrystal. In the amyloid structure (a), kinetic energy from axial stress wave is dissipated into transverse bending mode motion of the overall fibril only. While in the silk nanocrystal (b), out-of-phase motions of the beta strands in the transverse x and y directions (c) provide additional energy dissipation channels. The local motion shown in panel (c) is defined as the relative displacement between one protofibil and the average value in each layer. The snapshots in panel (c) illustrate beamlike vibrations of the amyloid fibril, and much larger and more erratic interstrand fluctuations in silk nanocrystals.

to dissipate kinetic energy from external impacts efficiently, as featured in the great impact resistance of spiders' capture web that effectively converts kinetic energy brought by caught insects into heat. This feature is not available in conventional materials with strong interatomic bonds, such as steel or glass, and even carbon nanotubes. Whereas these materials feature a great level of strength, their capacity to dissipate energy is limited. Simulation results of WFT in carbon nanotubes (results not shown) reveal that during the time scales shown in Fig. 2, there is no noticeable energy dissipation, and thus the damping coefficient (which is not well defined by the fitting procedure in this case due to the extremely small slope) is several orders of magnitudes larger than those we have identified here for fibrous proteins.

IV. CONCLUSION

In summary, we carried out a systematic study of the mechanical energy transfer process in fibrous beta-sheet-rich proteins, all featuring highly ordered H-bond networks. Our work goes beyond earlier efforts that focused on purely elastic constants, and elucidates the capacity of these protein materials to dissipate mechanical energy. We find that all beta-sheet-rich protein fibrils have excellent mechanical properties, where the measured Young's moduli on the order of 20–40 GPa are comparable to widely used engineering materials such as concrete and glass [30]. A network model reveals that these mechanical properties can be related to the effective properties of H bonds, which also explains the observed stiffness variations with respect to their molecular structures. Silk nanocrystals are found to have the highest Young's modulus, reaching close to 40 GPa.

Upon dynamical loading, we find that mechanical energy waves propagate at a high speed of several km/s. However,

we find significant differences in the capacity of the protein fibrils to dissipate mechanical energy. Specifically, our results show that the quasi-two-dimensional lattice found in silk nanocrystals efficiently improves energy dissipation capacity manifold compared to amyloids or beta solenoids. This is remarkable in particular in light of the finding that silk nanocrystals are also the structures with the greatest modulus, suggesting that this particular protein structure combines both exceptional stiffness and exceptional energy dissipation capacity. This behavior was explained by intrastrand fluctuations in transverse directions that give rise to an efficient dissipation channel toward heat.

It should be noted that our work is focused solely on small deformation and the elastodynamic regime. Under elevated loads exceeding the intrinsic strength of hydrogen bonds [11,26], sacrificial bond breaking provides another mechanism to dissipate kinetic energy [27], by making use of breaking and self-healing of the noncovalent hydrogen bond network. Those examples can be found in capture silks [28], wood [29], and bone [30]. The basic understanding developed from our studies provides guidelines for novel peptide-based material and multifunctional nanodevice designs [31,32], featuring high stiffness, strength, and impact resistance. This could perhaps be achieved by combining carbon

nanostructures such as graphene or carbon nanotubes with protein domains such as silk nanocrystals. Moreover, the energy transfer and dissipation mechanisms discussed here could also help one to understand thermal management issues in biological systems [33,34].

ACKNOWLEDGMENTS

[1] J. C. M. van Hest and D. A. Tirrel, Chem. Commun. **19**, 1897 (2001)

[2] C. E. MacPhee and D. N. Woolfson, Curr. Opin. Solid State Mater. Sci. **8**, 141 (2004).

[3] C. E. MacPhee and C. M. Dobson, J. Am. Chem. Soc. **122**, 12707 (2000).

[4] J. F. Smith *et al.*, Proc. Natl. Acad. Sci. U.S.A. **103**, 15806 (2006).

[5] S. Keten *et al.*, Cell. Mol. Bioeng. **2**, 66 (2009).

[6] I. Krasnov, I. Diddens, N. Hauptmann, G. Helms, M. Ogurreck, T. Seydel, S. S. Funari, and M. Muller, Phys. Rev. Lett. **100**, 048104 (2008).

[7] C. L. Craig, *Spiderwebs and Silk: Tracing Evolution from Molecules to Genes to Phenotypes* (Oxford University Press, New York, 2003).

[8] P. R. LeDuc and D. N. Robinson, Adv. Mater. **19**, 3761 (2007).

[9] N. Du *et al.*, Biophys. J. **91**, 4528 (2006).

[10] S. M. Lee *et al.*, Science **324**, 488 (2009).

[11] S. Keten and M. J. Buehler, Nano Lett. **8**, 743 (2008).

[12] D. J. Brockwell *et al.*, Nat. Struct. Mol. Biol. **10**, 731 (2003).

[13] H. Kolsky, *Stress Waves in Solids* (Dover, New York, 1963).

[14] N. H. Fletcher, *The Chemical Physics of Ice* (Cambridge University Press, New York, 1970).

[15] R. Paparcone, J. Sanchez, and M. J. Buehler, J. Comput. Theor. Nanosci. **7**, 1279 (2009).

[16] R. Paparcone and M. J. Buehler, Appl. Phys. Lett. **94**, 243904 (2009).

[17] A. M. Lesk, *Introduction to Protein Science* (Oxford University Press, New York, 2004).

[18] Y. Termonia, Macromolecules **27**, 7378 (1994).

[19] L. F. Drummy, B. L. Farmer, and R. R. Naik, Soft Mater. **3**, 877 (2007).

[20] T. Lazaridis and M. Karplus, Science **278**, 1928 (1997).

[21] T. Lazaridis and M. Karplus, Proteins **35**, 133 (1999).

[22] E. Paci and M. Karplus, Proc. Natl. Acad. Sci. U.S.A. **97**, 6521 (2000).

[23] W. L. Jorgensen *et al.*, J. Chem. Phys. **79**, 926 (1983).

[24] T. P. Knowles *et al.*, Science **318**, 1900 (2007).

[25] Z. Xu, R. Paparcone, and M. J. Buehler, Biophys. J. **98**, 2053 (2010).

[26] S. Keten and M. J. Buehler, Phys. Rev. Lett. **100**, 198301 (2008).

[27] S. Keten *et al.*, Nat. Mater. **9**, 359 (2010).

[28] N. Becker *et al.*, Nat. Mater. **2**, 278 (2003).

[29] J. Keckes *et al.*, Nat. Mater. **2**, 810 (2003).

[30] G. E. Fantner *et al.*, Nat. Mater. **4**, 612 (2005).

[31] M. Reches and E. Gazit, in *Nanomaterials Chemistry: Novel Aspects and New Directions*, edited by C. N. R. Rao, A. Mueller, and A. K. Cheetham (Wiley-VCH, Weinheim, 2007), p. 171.

[32] M. Buehler, Nat. Nanotechnol. **5**, 172 (2010).

[33] K. Moritsugu, O. Miyashita, and A. Kidera, Phys. Rev. Lett. **85**, 3970 (2000).

[34] D. M. Leitner, Phys. Rev. Lett. **87**, 188102 (2001).